THE ASTROPHYSICAL JOURNAL, 492:L121–L124, 1998 January 10

UNVEILING THE HIDDEN NUCLEUS OF IC 5063 WITH NICMOS

V. P. KULKARNI,[1] D. CALZETTI,[2] L. BERGERON,[2] M. RIEKE,[1] D. AXON,[2,3] C. SKINNER,[2,3,4] L. COLINA,[2,3] W. SPARKS,[2] D. DAOU,[2] D. GILMORE,[2] S. HOLFELTZ,[2] J. MACKENTY,[2] K. NOLL,[2] C. RITCHIE,[2] G. SCHNEIDER,[1] A. SCHULTZ,[2] A. STORRS,[2] A. SUCHKOV,[2] AND R. THOMPSON[1]

Received 1997 July 31; accepted 1997 October 30; published 1997 December 30

ABSTRACT

We present high-resolution near-infrared images of the Seyfert 2 galaxy IC 5063 obtained using the Near-Infrared Camera and Multiobject Spectrometer (NICMOS) in broadband filters at 1.1, 1.6, and 2.2 μm (FWHM $\approx$ 0.″21 at 2.2 μm). The images show a very red, unresolved point source at the center of the galaxy, confirming the existence of the obscured active nucleus inferred from previous ground-based studies. The 2.2 μm flux, supplemented with ground-based L'-band observations, suggests thermal emission equivalent to a blackbody at a temperature of 720 K. We ascribe the emission not to direct light from the nucleus, but to hot dust in the inner part of the torus. The 1.6 μm emission is only minimally affected by the hot dust emission. The luminosity of the central source producing most of the 1.6 μm emission, not corrected for extinction, is 1.5×10^{41} ergs s^{-1}, integrated over the F160W filter only.

We also present lower spatial resolution images of IC 5063 obtained with NICMOS in the emission lines of [Fe II] λ1.644 μm, Paα λ1.8756 μm, and H_2 λ2.1218 μm. These images reveal a linear emission morphology comprised of two bright knots, separated by 1.″8 on either side of a central knot that is at the location of the continuum nucleus. A comparison with high-resolution radio continuum maps shows that there is a one-to-one spatial correspondence between the radio lobes and the emission-line knots, directly implying that the [Fe II] and H_2 emission is created by fast shocks produced by the advancing radio jets. The asymmetry in the [Fe II]/H_2 ratio may suggest a difference in either the shock velocities or the molecular mass on the two sides of the nucleus.

Subject heading: galaxies: individual (IC 5063) — galaxies: nuclei

1. INTRODUCTION

The unified model (Antonucci 1993) for active galactic nuclei (AGNs), in which our viewing angle regulates whether we see a narrow-line (Seyfert 2) or broad-line (Seyfert 1) object, has risen to prominence because of two key observational results: (1) the detection of scattered, broad Balmer lines and blue continuum in ostensively narrow-line galaxies (e.g., Antonucci & Miller 1985; Young et al. 1996a), and (2) the "ionization cone" morphology of the circumnuclear emission-line regions (Unger et al. 1987; Wilson & Tsvetanov 1994). In this picture, the aspect angle dependence is created by the presence of an optically thick torus that obscures the active nucleus and the broad-line region, yielding a Seyfert 2 galaxy, except when viewed close to its polar axis. X-ray studies imply that in many objects, the obscuring column density exceeds $\gtrsim 10^{22}$ cm^{-2}. Further support for this model has come from optical imaging and polarimetry (e.g., Capetti et al. 1995a, 1995b, 1996) with the *Hubble Space Telescope* (*HST*), which has shown that in Seyfert 2 galaxies, the nucleus is invariably hidden behind a central dust lane.

Ground-based near-IR studies of many galaxies have revealed a highly polarized nuclear region (Packham et al. 1996; Young et al. 1996a). With ground-based resolutions, it is not possible to decide whether the polarized infrared source is compact and formed by dichroic extinction of hot dust located in the torus (Young et al. 1996a) or whether it is simply an extended scattering zone that, at optical wavelengths, is obscured by foreground dust.

Continuum imaging in the infrared at *HST* resolutions could conceivably provide a method of distinguishing between these two explanations by establishing the size of the near-IR–emitting zone. Another important problem in which *HST* infrared imaging is critical is in determining the origin of the strong [Fe II] emission observed in the narrow-line region (NLR) of Seyfert galaxies (Forbes & Ward 1993; Blietz et al. 1994; Simpson et al. 1996) that may be caused by photoionization by the nucleus or by strong shocks created by the ejected radio plasma (either collisionally or by radiation produced from the shocks). *HST* optical emission line imagery (e.g., Capetti et al. 1995a, 1995b, 1996; Capetti, Axon, & Macchetto 1997; Bower et al. 1994) and spectroscopy (Winge et al. 1997; Axon et al. 1997) have recently provided compelling evidence that both the morphology and the kinematics of the NLR are dictated by the interaction between ejected, radio-emitting material and the ambient gas. Demonstrating that the spatial structure of the [Fe II] emission is also strongly related to that of the radio emission would provide substantive support for the shock excitation model.

The nearby ($z = 0.0110$) S0 galaxy IC 5063 (PKS 2048−572) is an ideal candidate in which to address both these issues. Not only is IC 5063 one of the strongest radio sources among the Seyfert galaxies, with a luminosity at 1.4 GHz about 2 orders of magnitude higher than a typical Seyfert galaxy (Ulvestad & Wilson 1984), but it also has a very red $K - L'$ color index in the inner 5″ (Axon, Bailey, & Hough 1982) and scattered broad Hα emission (Inglis et al. 1993), which suggests that it contains a hidden luminous source.

In this Letter, we present diffraction-limited, broadband near-infrared images of IC 5063 obtained with the Near-Infrared Camera and Multiobject Spectrometer (NICMOS) on board the

[1] Steward Observatory, University of Arizona, 933 North Cherry Avenue, Tucson, AZ 85721-0065.

[2] Space Telescope Science Institute, 3700 San Martin Drive, Baltimore, MD 21218.

[3] On assignment from the Space Sciences Division of the European Space Agency.

[4] Deceased.

HST (see, for example, Thompson, Rieke, & Schneider 1998 for details on the NICMOS instrument). These images allow us to probe through the foreground dust obscuration to the center of IC 5063 and enable us to provide important new constraints on the nature of the central luminous source. We also present narrowband NICMOS observations in the emission lines of [Fe II] λ1.644 μm, Paα λ1.875 μm, and H_2 λ2.122 μm, which reveal a direct spatial correspondence between the line and radio morphologies, and therefore provide strong evidence that the [Fe II] emission is created by shocks.

Throughout this Letter, we adopt $H_0 = 50$ km s^{-1} Mpc^{-1}, so that $1'' = 0.32$ kpc at the redshift of IC 5063.

2. OBSERVATIONS AND DATA REDUCTION

All observations were obtained between 1997 April 18, UT 19:57, and April 19, UT 02:30. Images were taken with NICMOS camera 2 in filters (central wavelength and FWHM in parentheses) F110W (1.100 and 0.592 μm), F160W (1.594 and 0.403 μm), and F222M (2.216 and 0.143 μm). Two images each were taken in filters F110W and F160W, to allow optimal cosmic-ray (CR) removal. Six beam-switched images with a chop throw of 119″ were obtained in F222M and combined to reject CRs and subtract the thermal background from the telescope and NICMOS foreoptics. Each exposure comprised a number of logarithmically spaced nondestructive reads, which were optimally combined to correct for pixel saturation and CR hits. The total exposure times in the on-target images were 512 s each for F110W and F160W and 768 s for F222M. The image plate scale for camera 2 was 0.″076 pixel^{-1}, giving a 19.″4 × 19.″4 field of view. The FWHM of the point-spread function (PSF) for camera 2 at the time of our observations was 0.″21 (i.e., 2.7 pixels) at 2.2 μm.

Broadband continuum images were also obtained using NICMOS camera 3 in the same filters. In addition, emission-line images were obtained with camera 3 using narrowband filters F166N (1.658 and 0.0164 μm), F190N (1.900 and 0.0174 μm), and F215N (2.149 and 0.020 μm), which, for IC 5063, encompass the redshifted emission lines from [Fe II] λ1.644 μm, H I Paα λ1.8756 μm, and H_2 λ2.1218 μm. The F190N, F215N, and F222M exposures were beam-switched as for the camera 2 F222M exposures. The total exposure times in the on-target observations were 64 s for F110W, 128 s for F160W, 192 s for F222M, and 1024 s each for F166N, F190N, and F215N. The plate scale for camera 3 images was 0.″204 pixel^{-1} with a field of view of 52.″2 × 52.″2. Due to the inability of the NICMOS internal mechanism to reach the optimal camera 3 focus at the time of observation, the point-spread function for these images was unfortunately degraded to ≈0.″7 at 1.6 μm. Nevertheless, capitalizing on the elimination of the highly variable, bright OH sky background, which limits ground-based narrowband observations in the near-IR, they yield important new information on the morphology of the emission-line regions.

The images were reduced using the IRAF/STSDAS task CALNICA developed for the calibration of NICMOS images at the Space Telescope Science Institute. CALNICA performs the following steps: bad pixel masking, bias subtraction, dark current subtraction, correction for detector nonlinearity, flat-field correction, linear regression to the individual reads to extract count rates, and correction for cosmic rays and pixel saturation. With the exception of the F110W in camera 2 for which we used a preliminary on-orbit flat, we used prelaunch flats for flat-fielding. Similarly, the bad pixel masks and detector nonlinearity corrections were based on prelaunch data. Individual on-target exposures were averaged. In cases where the beam-switched "sky" images were taken, these were also averaged to produce "sky" images that were subtracted from the average object images. The sky subtraction yielded quite smooth images, with negligible residual differences across the images. Finally, any remaining bad pixels or cosmic rays were cleaned by linearly interpolating across them based on values in the neighboring pixels.

Absolute flux calibration was done using the observations of standard star P330E that were performed during the Servicing Mission Observatory Verification (SMOV) program. We expect the uncertainty in the absolute photometry to be ≈10%–15%. The zero points of the magnitude scales are based on Campins, Rieke, & Lebofsky (1985).

3. RESULTS

3.1. *Continuum Images: Near-IR Colors of the Obscured Nucleus*

Figure 1*a* (Plate L21) shows the central 12.″1 × 12.″1 of the final camera 2 images in F110W (*upper left panel*), F160W (*upper right panel*), and F222M (*lower left panel*). The F222M image is dominated by the presence of a very bright, unresolved nuclear source with a FWHM of 2.7 pixels (0.″21), which shows the first Airy ring at a radial distance of ≈4 pixels (≈0.″30), i.e., the image is diffraction-limited. The F222M nuclear source has a PSF nearly identical to the expected PSF produced with the Tiny Tim software. The resulting upper limit on the size (FWHM) of the source is $\lesssim 66(H_0/50)^{-1}$ pc.

In order to estimate the colors of the central point source, we first subtracted the contribution of the underlying galaxy using a synthetic model generated by isophotal fitting with the ISOPHOTE package in IRAF/STSDAS. The radial profiles used in generating the galaxy models shown in Figure 2 are well described by an $r^{1/4}$ law, except in the very center where the point source is important. To remove the underlying galaxy contribution from the central region, we fixed the flux at the center of each image to the value at a radius of 7.5 pixels from the nucleus; this yields colors of the underlying galaxy of $m_{\rm F160W} - m_{\rm F222M} = 0.25$ and $m_{\rm F110W} - m_{\rm F160W} = 1.24$, fairly representative of a typical elliptical galaxy. Figure 1*b* (Plate L22) shows the central 3″ × 3″ regions of the images in filters F110W (*upper left panel*), F160W (*upper right panel*), and F222M (*lower left panel*) after galaxy subtraction.

Aperture photometry was carried out on the nuclear images using an aperture of 12 pixels radius. The fluxes of the central source are ≤0.0067 Jy (≥16.1 mag) in F110W, 0.00145 Jy (14.68 mag) in F160W, and 0.00477 Jy (12.86 mag) in F222M. The largest contribution to the uncertainty in the photometry of the central source comes from the underlying galaxy subtraction; this uncertainty is of the order of 20% in the F222M band, and increasingly larger at bluer wavelengths because of the decreasing contrast between the emission from the galaxy and the emission from the central source. Indeed, the galaxy-subtracted nuclear image in the F110W band is resolved, unlike the other two bands, and the different behavior is not accounted for by the different diffraction limits between the three bands. Thus, the residual contribution from the underlying galaxy may be a major component of the measured nuclear flux in the F110W band; therefore, its value is given as an upper limit.

The increasingly red colors for longer wavelengths,

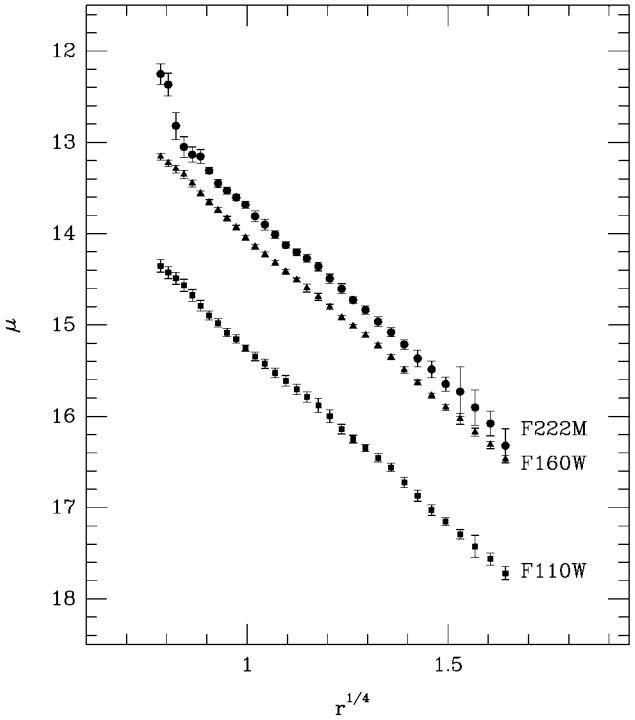

FIG. 2.—Radial profiles used in generating the fits used for the galaxy stellar light in NICMOS camera 2 images of IC 5063 in F110W, F160W, and F222M; μ is in units of magnitudes per square arcsecond, and r is in arcseconds.

$m_{\rm F160W} - m_{\rm F222M} = 1.82$ and $K - L' = 2.15$ (Axon et al. 1982), suggest that both the F222M and the L' fluxes are dominated by emission from hot dust heated by the nuclear source. The corresponding blackbody temperature inferred from the F222M and L' bands is $T_d \simeq 720$ K. The L' flux for the nuclear source alone was derived from the 5″ aperture value of Axon et al. (1982) by taking the F222M value for the galaxy alone in that size aperture and scaling it by $K - L' \approx 0.2$. The galaxy flux at L' corresponds to 24% of the total L' flux in 5″. The high-temperature T_d and the unresolved F222M emission indicate that we are observing hot dust in the molecular torus surrounding the central source, as in other nearby AGNs (e.g., NGC 1068—see Young et al. 1996b).

Approximately 75% of the F160W nuclear flux is not from the hot dust producing the F222M and L' fluxes. If this flux is from the nuclear source itself, it must be intrinsically blue with no more than $A_V \sim 15$ mag of extinction or else the nuclear flux would dominate at 2.2 μm and longer wavelengths. The F160W nuclear flux, not corrected for extinction, is 1.5×10^{41} ergs s^{-1}, integrated over the F160W filter only. This is comparable to other AGNs but leaves open the question of the exact nature of the F160W nuclear flux.

Figures 3*a* and 3*b* (Plates L23 and L24) show color maps of IC 5063 in F110W–F222M and F160W–F222M, respectively. A complex system of dust lanes similar to the outer dust lanes seen in the ground-based data of Colina, Sparks, & Macchetto (1991) is evident, running roughly parallel to the major axis of the galaxy. Typical values of $m_{\rm F110W} - m_{\rm F222M}$ and $m_{\rm F160W} - m_{\rm F222M}$ in these lanes are about 1.7 and 0.4, with an estimated uncertainty of about 0.2 mag. If we assume that an unreddened elliptical should have $J - K$ of 1.27 and $H - K$ of 0.24 (Frogel et al. 1978), then this implies $A_V \approx 2.5$ in the dust lanes, considerably larger than in the outer dust lanes whose average is $A_V = 0.3$ (Colina et al. 1991). Using the typical correlation between H column density and dust extinction in the Galactic interstellar medium, this would imply $N({\rm H}) \approx 5 \times 10^{21}$.

We note that there are about 10 small objects in the F110W and F160W images, each about 2–4 pixels wide. A few of these are visible in the 12.″1 × 12.″1 regions shown in the upper panels of Figure 1*a*. They have an $m_{\rm F110W} - m_{\rm F160W}$ color of ≈1.2, while the only object also visible in F222M (the brightest one) has $m_{\rm F160W} - m_{\rm F222M} = 0.26$. These colors are consistent with those of globular clusters; we therefore speculate that, as in Arp 220 (Scoville et al. 1998), these are globular clusters formed in a recent burst of star formation, perhaps also triggered by a merger.

3.2. *Emission-Line Regions*

The panels in Figure 4*a* (Plate L25) show the central 8.″4 × 8.″4 regions of the F166N (*upper left*), F190N (*upper right*), and F215N (*lower left*) images. Monochromatic line images (Fig. 4*b* [Pl. L26]) were created by masking out the central 25 lines of the images that encompass the regions with obvious line emission (seen in Fig. 4*a*), in both the narrow and wide filters, and by normalizing the remaining broadband image to the remaining narrowband image count rate and subtracting. Apart from the nuclear region of the H_2 image (Fig. 4*b*, *lower left panel*), where the extreme red color of the continuum source leads to oversubtraction, the subtraction is good.

The bright emission-line structures of both [Fe II] and Paα consist of three well-resolved knots aligned roughly linearly along the major axis of the galaxy. The central of the three knots is coincident with the bright point source detected in F222M that we assume to be the nucleus. The separation between the other two knots and the nucleus is ≈1.″8. In H_2, only the nucleus and the western knot are visible. The apparent displacement of the nuclear H_2 emission is probably an artifact of the poor continuum subtraction. The structure observed is closely similar to that seen in the ionized gas at optical wavelengths (Colina et al. 1991). The 8 GHz radio continuum map of Morganti, Oosterloo, & Tsvetanov (1997) from the Australia Telescope Compact Array (ATCA) shows a triple linear structure along P.A. = 295° (see Fig. 4*b*, *lower right panel*). The position angle of the radio axis is approximately perpendicular to that of the optical polarization (Inglis et al. 1993), in agreement with the predictions of the unified scheme. A comparison between the emission-line and radio images shows that there is a direct correspondence between the positions of the three emission-line knots and the three radio components (P.A. alignment to ≈1°), implying that they are physically related.

Outside this central region, the Paα shows more diffuse emission with an X-shaped structure with a total extent of ≈3 kpc, which is reminiscent of the much larger scale (22 and 6.4 kpc along its major and minor axes, respectively) X-shaped ionization structure seen in maps of [O III]/Hα ratio (Colina et al. 1991). This high-ionization X circumscribes the boundaries of the radio emission, suggesting to us that the covering factor is less along these directions compared with along the radio axis. Whereas the large-scale optical X structure might be a consequence of the absence of gas, inspection of the [O III] image shows that this is not the case for the region in which the Paα shows a similar morphology. This morphology can be explained if, for example, the covering factor of the compressed

gas on the radio axis is sufficient to attenuate the ionizing photons, and if a relatively unattenuated radiation field is leaking around the sides of the radio structure. Alternatively, the radiation field might be intrinsically anisotropic, i.e., the AGN may emit a hollow radiation cone.

It is well established that strong [Fe II] or H_2 lines trace shocks in supernova remnants and young stellar outflows. The study of Moorwood & Oliva (1988) shows that [Fe II] is also strong in starburst galaxies and is best explained as a consequence of supernova explosions. Imaging of the [Fe II] emission in NGC 1068 (Blietz et al. 1994) revealed extended structure cospatial with its radio jet, and this led them to suppose that it was formed by fast shocks created by the jet. Recent ground-based spectroscopy (Simpson et al. 1996 and references therein) has provided further evidence that [Fe II] is strong in Seyfert galaxies with linear radio sources. The [Fe II] $\lambda 1.64$ μm line originates from a level at $\sim 10^4$ K above the ground energy level, which can be populated in shock-heated gas or in gas photoionized by an AGN-type ionizing continuum. The models of Simpson et al. show that, in practice, it is hard to distinguish these two possibilities simply on the basis of the observed emission-line ratios.

The ratios of the line fluxes in the three regions in IC 5063 were obtained by aperture photometry. The [Fe II]/Paα line ratio is 0.26 in the eastern knot, 0.39 in the western knot, and 0.12 in the central region. The value of 0.12 observed in the central region is somewhat lower, but after correction for the reddening derived in § 3.1, it is about a factor of 2 larger, bringing the ratio into line with the values on the two knots. These values are very similar to those typically seen in the Seyfert sample of Forbes et al. The alignment of the radio and the
[Fe II] regions and the direct correspondence between the [Fe II] and radio hot spots strongly suggest that shocks associated with the radio jet are playing a formative role in the excitation of all three knots rather than just photoionization by the nucleus. Further support for this interpretation is provided by the strong H_2 on the western lobe.

There is a large difference between the [Fe II]/H_2 line ratio on the two knots, 6.9 in the eastern knot and 1.8 in the western knot. The weakness of the H_2 on the eastern side could be explained by a variety of means. The color maps (Figs. 3*a* and 3*b*) do not reveal any significant differences in reddening between the regions near the emission-line knots on the two sides of the nucleus; this rules out differential reddening as an explanation. The asymmetry may be explained by either an excess of molecular gas on the western side (for example, the jet may have struck a molecular cloud) or a difference in the shock speeds on either side. In support of the first of these suggestions, Morganti et al. (1997) report the presence of strong H I absorption in front of the western radio knot. Within a factor of a few, the H I column density they measure is the same as what we derive from the color maps (§ 3.1). For the alternative explanation to be viable, the shocks would have to be fast enough to dissociate H_2 on the eastern side, but not on the western side. The velocity structure seen by Morganti et al. (1997) argues against this explanation.

4. CONCLUSIONS

We have obtained deep images of the galaxy IC 5063 with NICMOS. We have detected a very red point source [FWHM $\lesssim 66(H_0/50)^{-1}$ pc] at the center of this galaxy, which is consistent with previous suggestions that this galaxy harbors a dust-obscured active nucleus. These observations provide further support to the unified theory of active galactic nuclei. The 2.2 μm flux is dominated by thermal emission from dust at a temperature of 720 K; the emission probably originates from the dusty molecular torus surrounding the nucleus. About 75% of the flux at 1.6 μm is due to emission other than hot dust; for this source, the intrinsic luminosity in the F160W band is $L_{1.6\,\mu\mathrm{m}} \simeq 1.5 \times 10^{41}$ ergs s^{-1}, not corrected for extinction. The observed luminosity is in agreement with typical values expected for AGNs.

Our NICMOS observations of IC 5063 have also revealed three emission-line regions in [Fe II], Paα, and H_2 located along the major axis in the central parts of this galaxy. The very good spatial alignment of these regions with the knots seen in radio emission suggests that the near-infrared line emission arises in shocks produced by the radio jets.

It is a pleasure to thank Rafaella Morganti for providing her radio map of IC 5063 and the related preprint prior to publication.

REFERENCES

Antonucci, R. R. J. 1993, ARA&A, 31, 473
Antonucci, R. R. J., & Miller, J. S. 1985, ApJ, 297, 621
Axon, D. J., Bailey, J., & Hough, J. H. 1982, Nature, 299, 234
Axon, D. J., Marconi, A., Macchetto, F. D., Capetti, A., & Robinson, A. 1997, Ap&SS, 248, 69
Blietz, M., Cameron, M., Drapatz, S., Genzel, R., Krabbe, A., van der Werf, P., Sternberg, A., & Ward, M. 1994, ApJ, 421, 92
Bower, G. A., Wilson, A. S., Mulchaey, J. S., Miley, G. K., Heckman, T. M., & Krolik, J. H. 1994, AJ, 107, 1686
Campins, H., Rieke, G. H., & Lebofsky, M. J. 1985, AJ, 90, 896
Capetti, A., Axon, D. J., Kukula, M., Macchetto, F., Pedlar, A., Sparks, W. B., & Boksenberg, A. 1995a, ApJ, 454, L85
Capetti, A., Axon, D. J., Macchetto, F., Sparks, W. B., & Boksenberg, A. 1996, ApJ, 466, 169
Capetti, A., Macchetto, F., Axon, D. J., Sparks, W. B., & Boksenberg, A. 1995b, ApJ, 448, 600
Capetti, A., Axon, D. J., & Macchetto, F. D. 1997, ApJ, 487, 560
Colina, L., Sparks, W. B., & Macchetto, F. 1991, ApJ, 370, 102
Forbes, D., & Ward, M. 1993, ApJ, 416, 150
Frogel, J. A., Persson, S. E., Aaronson, M., & Matthews, K. 1978, ApJ, 220, 75
Inglis, M. D., Brindle, C., Hough, J. H., Young, S., Axon, D. J., Bailey, J. A., & Ward, M. J. 1993, MNRAS, 263, 895
Moorwood, A., & Oliva, E. 1988, A&A, 203, 278
Morganti, R., Oosterloo, T., & Tsvetanov, Z. 1997, in ASP Conf. Ser. 113, Emission Lines in Active Galaxies: New Methods and Techniques, IAU Colloq. 159, ed. B. M. Peterson, F.-Z. Cheng, and A. S. Wilson (San Francisco: ASP), 310
Packham, C., Hough, J. H., Young, S., Chrysostomou, A., Bailey, J. A., Axon, D. J., & Ward, M. J. 1996, MNRAS, 278, 406
Scoville, N. Z., et al. 1998, ApJ, 492, L107
Simpson, C., Forbes, D. A., Baker, A. C., & Ward, M. J. 1996, MNRAS, 283, 777
Thompson, R. I., Rieke, M., & Schneider, G. 1998, ApJ, 492, L95
Ulvestad, J. S., & Wilson, A. S. 1984, ApJ, 285, 439
Unger, S., Pedlar, A., Axon, D. J., Whittle, M., Meurs, E. J. A., & Ward, M. J. 1987, MNRAS, 228, 671
Wilson, A., & Tsvetanov, Z. 1994, AJ, 107, 1227
Winge, C., Axon, D. J., Macchetto, F. D., & Capetti, A. 1997, ApJ, 487, L121
Young, S., Hough, J. H., Efstathiou, A., Wills, B. J., Bailey, J. A., Ward, M. J., & Axon, D. J. 1996a, MNRAS, 281, 1206
Young, S., Packham, C., Hough, J. H., & Efstathiou, A. 1996b, MNRAS, 283, L1

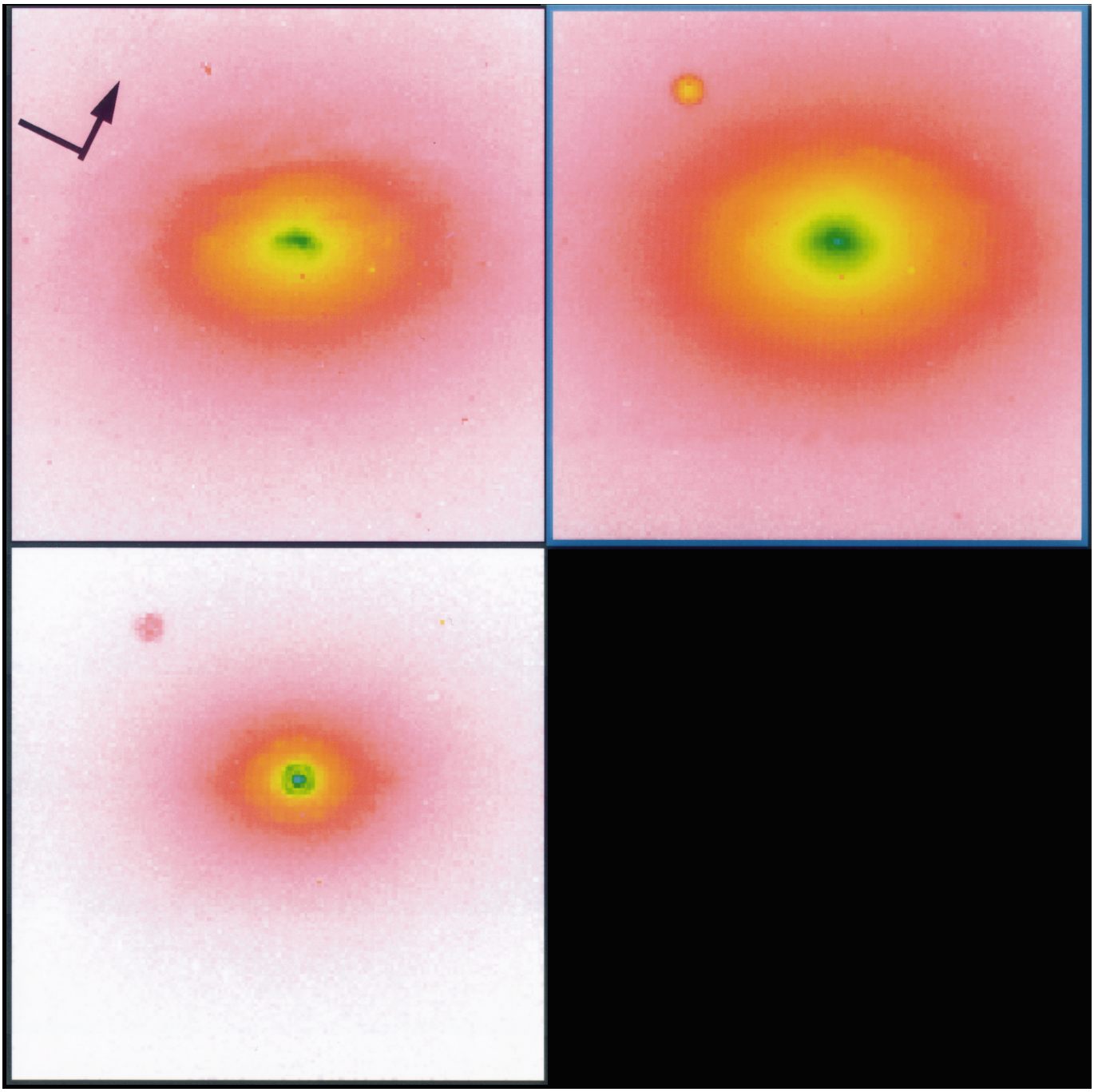

FIG. 1*a*

FIG. 1.—(*a*) Central 12″.1 × 12″.1 regions of the NICMOS camera 2 images of IC 5063 in F110W (*upper left*), F160W (*upper right*), and F222M (*lower left*). The image *y*-axis is 26°.58 east of north, as shown in the upper left panel (the arrow denotes north). The color scale is logarithmic. In the upper panels, green denotes the brightest regions, and pale pink or white denotes the faintest regions. In the lower left panel, blue denotes the brightest regions, and white denotes the faintest regions. The circular feature in the upper left-hand corner of the upper right and lower left panels is caused by the coronagraphic hole (this feature is not visible in the upper left panel because the flat used for F110W incorporated the coronagraphic hole). (*b*) Central 3″ × 3″ regions of the images after subtraction of the galaxy, showing the nuclear source in F110W (*upper left*), F160W (*upper right*), and F222M (*lower left*). The image *y*-axis is 26°.58 east of north, as shown in the upper left panel of (*a*). The color scale is logarithmic. White or bright yellow denotes the brightest regions, and dark brown denotes the faintest regions.

KULKARNI et al. (see 492, L122)

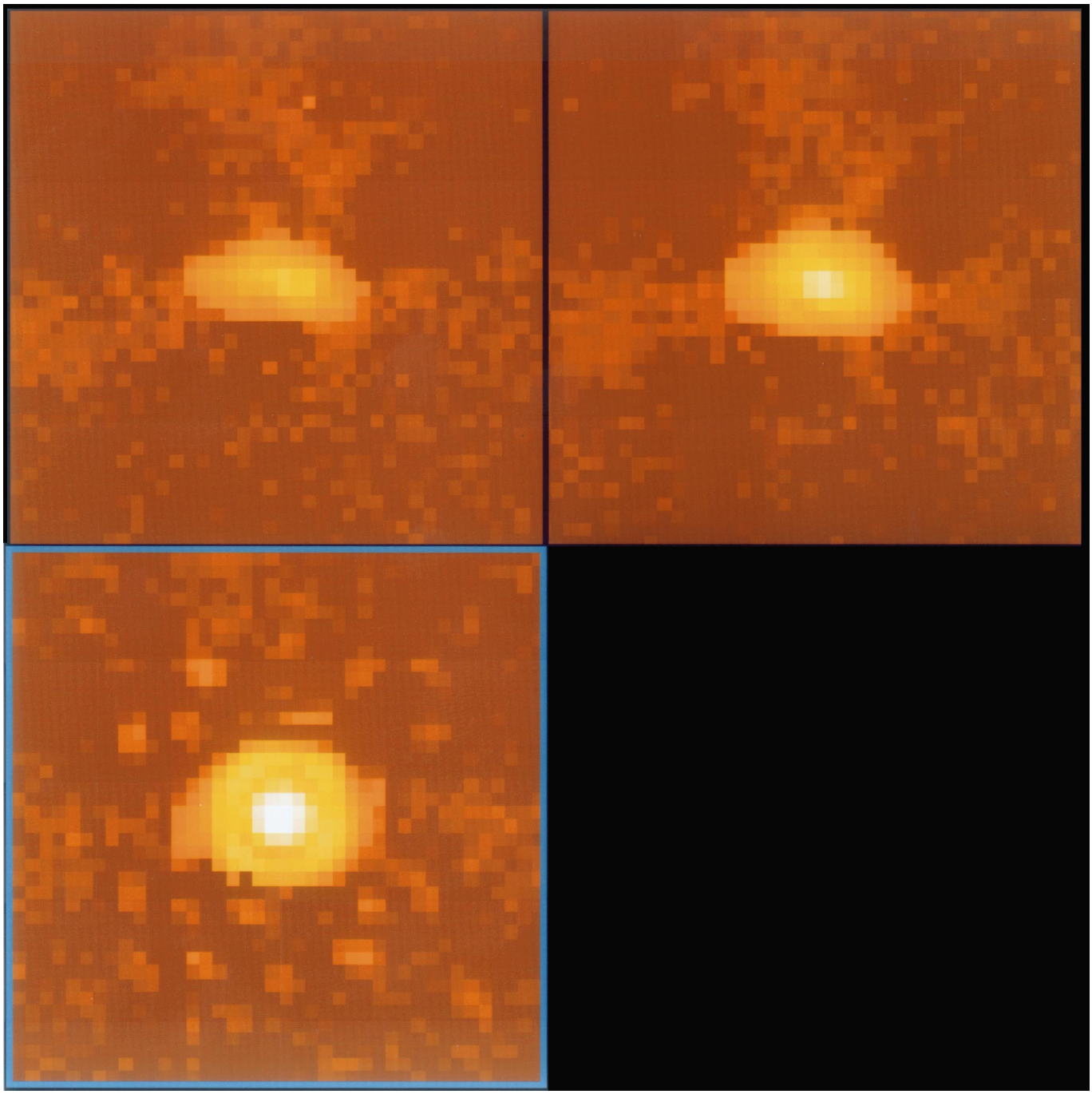

FIG. 1*b*

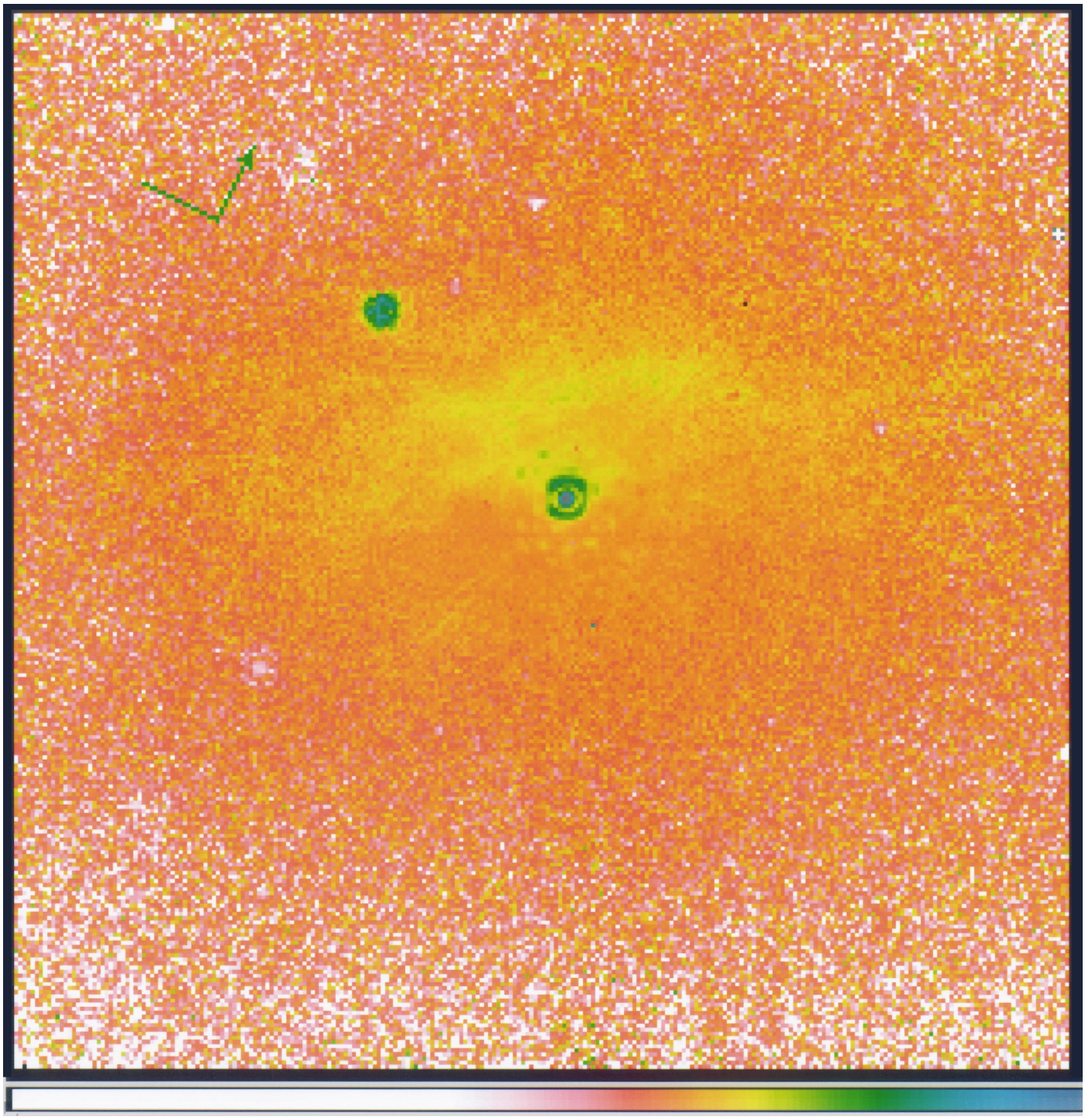

FIG. 3*a*

FIG. 3.—(*a*) Color map (entire 19.″4 × 19.″4) of IC 5063 in F110W–F222M. As in Fig. 1*a*, the coronagraphic hole is visible in the upper left quadrant. (*b*) Color map (entire 19.″4 × 19.″4) of IC 5063 in F160W–F222M. The image *y*-axis is 26.°58 east of north in each case, as shown (the arrow denotes north). The color scale in each case is linear and is shown at the bottom.

KULKARNI et al. (see 492, L123)

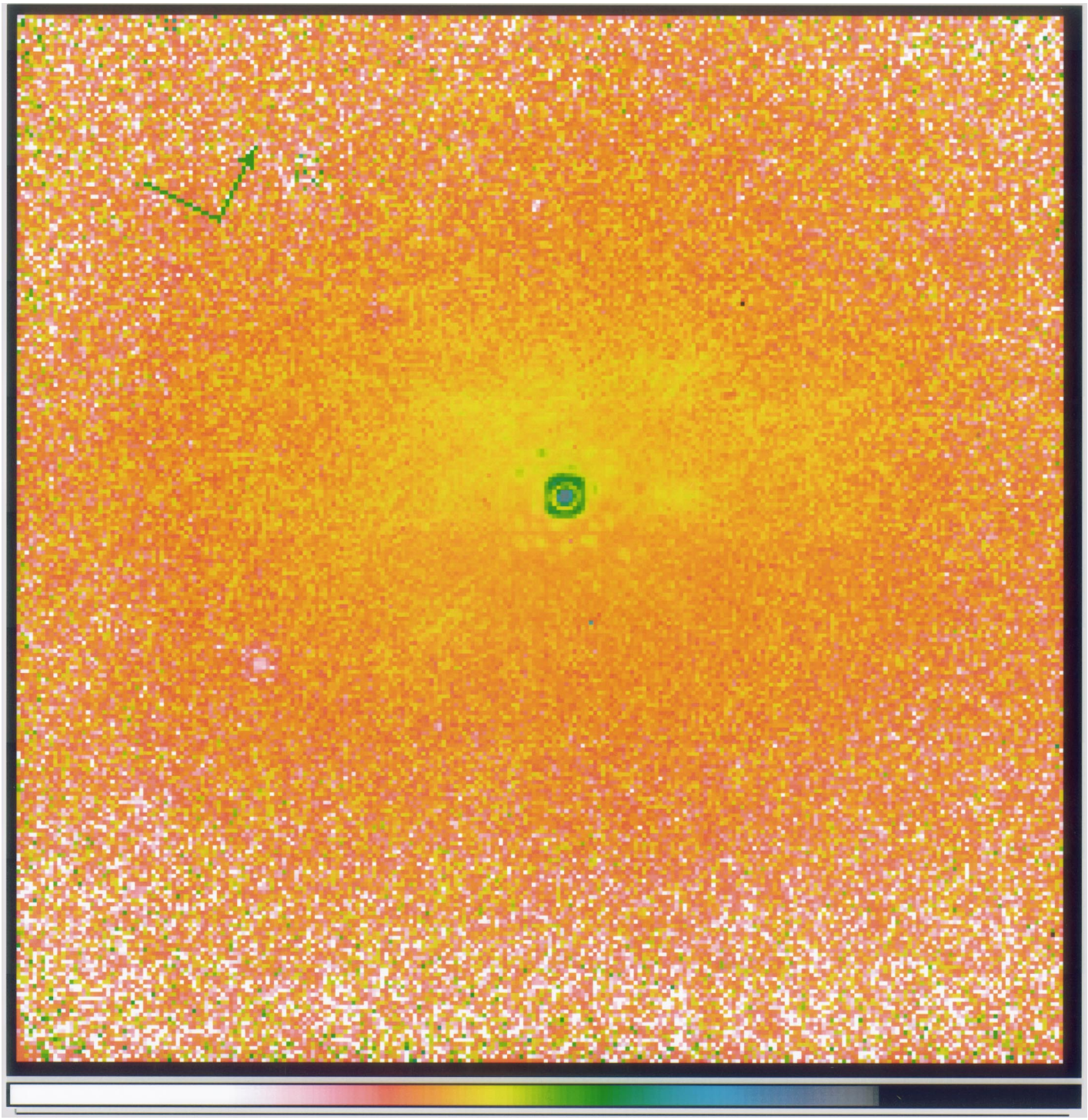

FIG. 3*b*

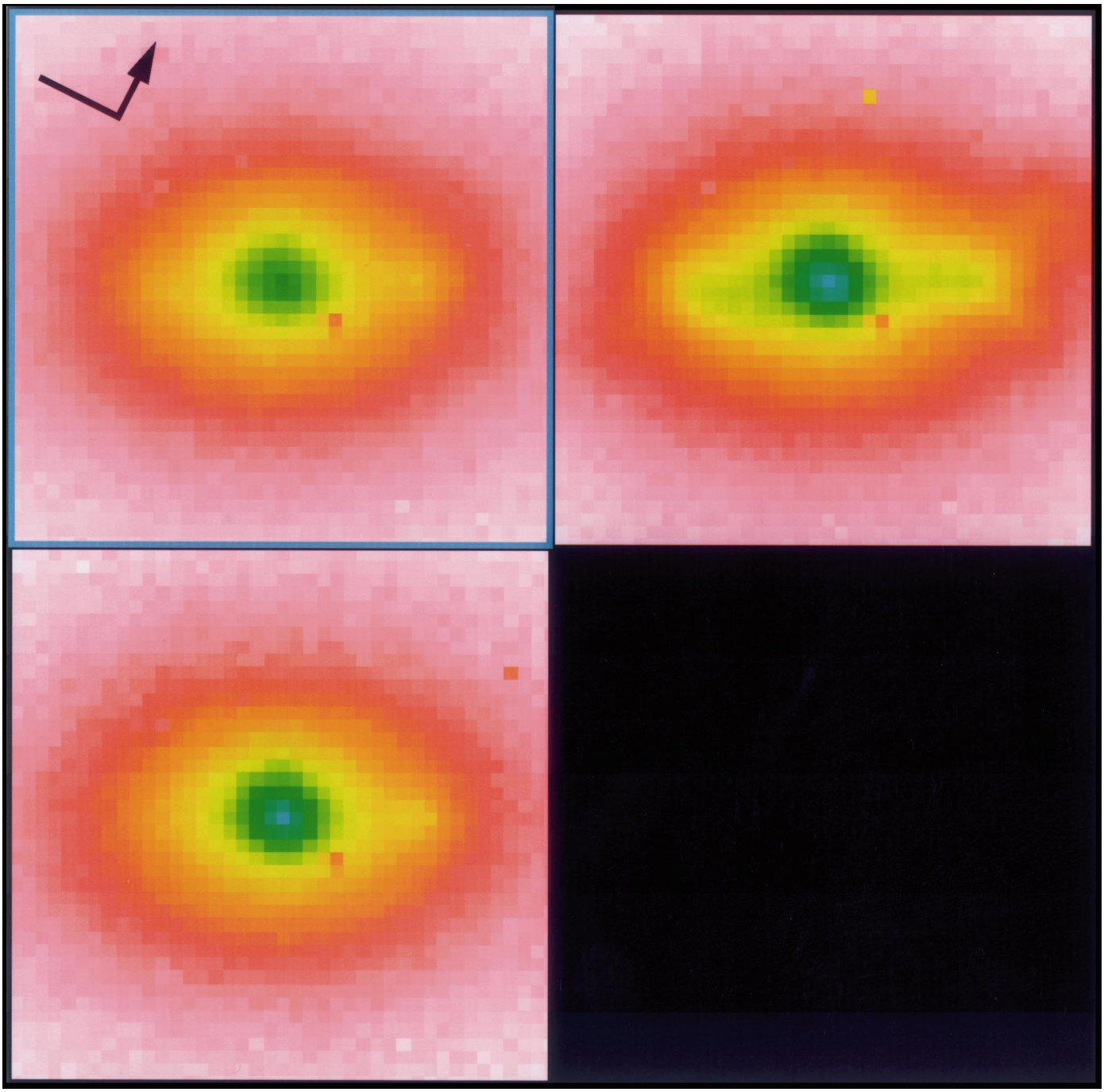

FIG. 4*a*

FIG. 4.—(*a*) Inner 8.″4 × 8.″4 regions of the NICMOS camera 3 images of IC 5063 in F166N (*upper left*), F190N (*upper right*), and F215N (*lower left*). The image *y*-axis is 27.°00 east of north, as shown in the upper left panel (the arrow denotes north). (*b*) Inner 8.″4 × 8.″4 regions of the images of IC 5063 in continuum-subtracted F166N (*upper left*), continuum-subtracted F190N (*upper right*), and continuum-subtracted F215N (*lower left*). The image *y*-axis is 27.°00 east of north, as shown in the upper left panel of (*a*) (the arrow denotes north). The color scale is logarithmic, with green or blue denoting the brightest level and pale pink denoting the faintest level. *Lower right panel*: inner 8.″4 × 8.″4 region of the ATCA 8 GHz radio continuum image from Morganti et al. (1997). The orientation is identical to that of the other panels. The color scale is logarithmic, with red denoting the brightest level and black denoting the faintest level. Most of the flux (195 mJy) comes from the NW knot. The beam shape is 1.″1 × 0.″8 elongated in P.A. = 51.°8. The resolution is 0.″3 pixel^{-1}. Note the clear similarity with the emission-line images in the other panels.

KULKARNI et al. (see 492, L124)

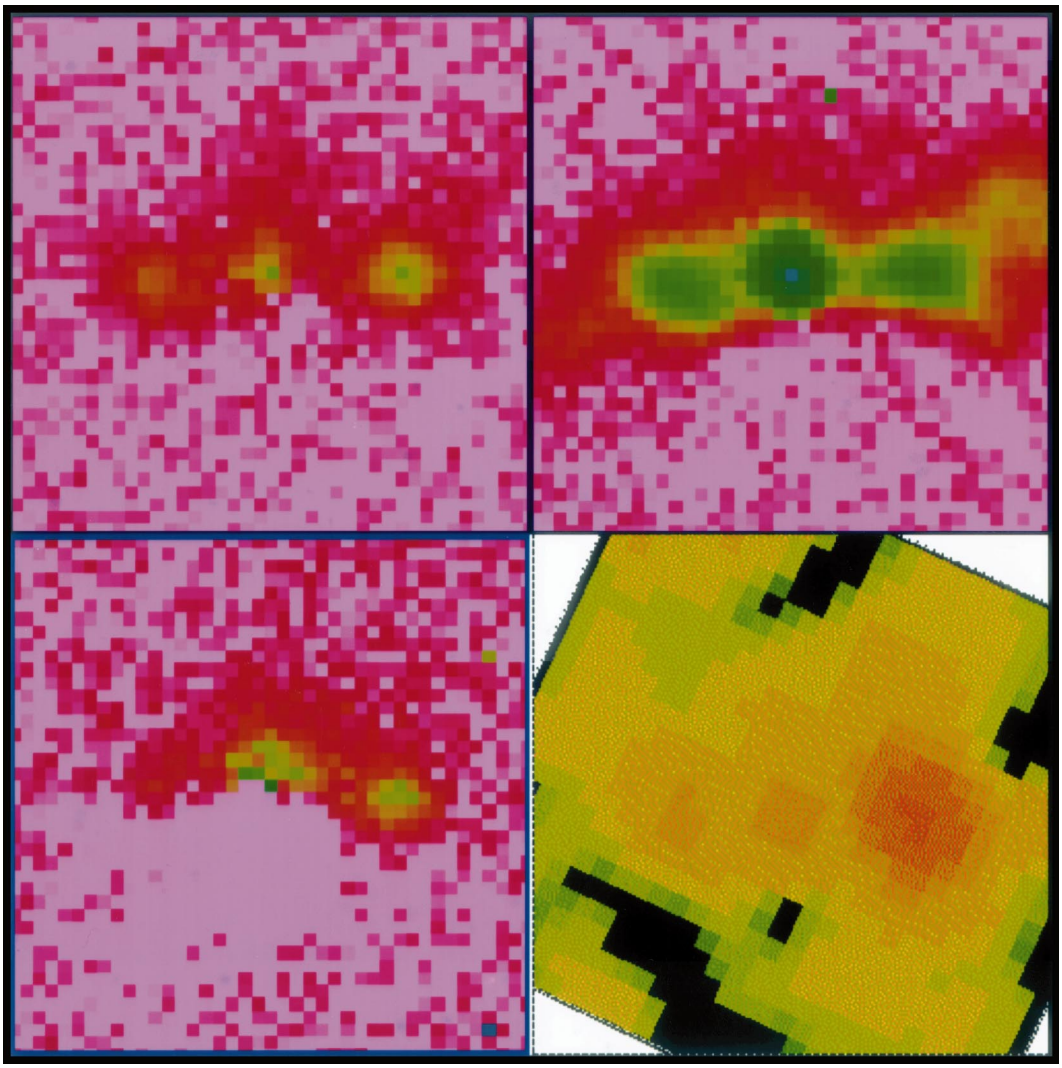

FIG. 4*b*

KULKARNI et al. (see 492, L124)